Key Points:
- A new type of polar cap patches, "polar cap hot patches," is identified to differentiate enhanced density structures from classical patches
- Hot patches are associated with particle precipitations, ion upflows, field-aligned currents, and shear flows in the polar cap
- Hot patches may lead to slightly stronger ionospheric scintillations of GNSS signals in the polar cap region than classical patches

Supporting Information:
- Supporting Information S1
- Movie S1
- Movie S2

Correspondence to:
Q.-H. Zhang,
zhangqinghe@sdu.edu.cn

Polar cap hot patches: Enhanced density structures different from the classical patches in the ionosphere

Q.-H. Zhang[1] [ID], Y.-Z. Ma[1], P. T. Jayachandran[2], J. Moen[3], M. Lockwood[4] [ID], Y.-L. Zhang[5], J. C. Foster[6] [ID], S.-R. Zhang[6] [ID], Y. Wang[1] [ID], D. R. Themens[2] [ID], B.-C. Zhang[7], and Z. Y. Xing[1] [ID]

[1]Shandong Provincial Key Laboratory of Optical Astronomy and Solar-Terrestrial Environment, Institute of Space Sciences, Shandong University, Weihai, China, [2]Physics Department, University of New Brunswick, Fredericton, New Brunswick, Canada, [3]Department of Physics, University of Oslo, Oslo, Norway, [4]Department of Meteorology, University of Reading, Reading, UK, [5]The Johns Hopkins University Applied Physics Laboratory, Laurel, Maryland, USA, [6]Haystack Observatory, Massachusetts Institute of Technology, Westford, Massachusetts, USA, [7]SOA Key Laboratory for Polar Science, Polar Research Institute of China, Shanghai, China

Abstract Based on in situ and ground-based observations, a new type of "polar cap hot patch" has been identified that is different from the classical polar cap enhanced density structure (cold patches). Comparing with the classical polar cap patches, which are transported from the dayside sunlit region with dense and cold plasma, the polar cap hot patches are associated with particle precipitations (therefore field-aligned currents), ion upflows, and flow shears. The hot patches may have the same order of density enhancement as classical patches in the topside ionosphere, suggesting that the hot patches may be produced by transported photoionization plasma into flow channels. Within the flow channels, the hot patches have low-energy particle precipitation and/or ion upflows associated with field-aligned currents and flow shears. Corresponding Global Navigation Satellite System (GNSS) signal scintillation measurements indicate that hot patches may produce slightly stronger radio signal scintillation in the polar cap region than classical patches. A new type of polar cap patches, "polar cap hot patches," is identified to differentiate enhanced density structures from classical patches. Hot patches are associated with particle precipitations, ion upflows, field-aligned currents, and shear flows in the polar cap. Hot patches may lead to slightly stronger ionospheric scintillations of GNSS signals in the polar cap region than classical patches.

1. Introduction

Patches are very common phenomena in the polar cap ionosphere. They are normally defined as islands of high-density ionospheric plasma surrounded by background plasma of half the density [*Crowley*, 1996]. Classical polar cap patches are often recognized to be segmented from the high-density plasma region in the midlatitude ionosphere, where the plasma is produced through photoionization by solar EUV with and of low temperature. This solar EUV produced plasma is drawn into the polar cap by the ionospheric convection [*Knudsen*, 1974; *Lockwood and Carlson*, 1992; *Foster et al.*, 2005; *Carlson*, 1994, 2012; *Lockwood et al.*, 2005; *Moen et al.*, 2006; *Zhang et al.*, 2011, 2013a]. *Weber et al.* [1984] suggested that auroral particle precipitation is also one source of polar cap patches, and *MacDougall and Jayachandran* [2007] also suggested that plasma transport from the auroral precipitation regions actually dominates polar cap patch production. *Basu et al.* [1990] and *Crowley et al.* [2000] called the plasma structures "patches" when they appeared in the polar cap and "blobs" after they were out of the polar cap. *Oksavik et al.* [2015] found that the ionospheric irregularities, associated with the poleward moving auroral forms (PMAFs) around cusp region, may give rise to stronger disturbances for navigation signals than the polar cap patches. It has been observed that scintillation level of a polar cap patch significantly increases when the patch is driven into the auroral oval and becomes exposed to particle precipitation [*Jin et al.*, 2014, 2015, 2016; *Wang et al.*, 2016].

Zhang et al. [2011] used the terminology Poleward-Moving Plasma Concentration Enhancements (PMPCEs) to interpret the patches, and then *Zhang et al.* [2013a] divided the enhanced density structures observed in the cusp region into two types: Type L PMPCEs (Less dense but hot plasma structures produced by precipitation) and Type H PMPCEs (Higher density but cold plasma structures produced by segmentation from the dayside sunlit region). *Zou et al.* [2016] also reported that patches are also related to polar cap precipitation.

Hence, it is necessary to differentiate "patches" generated by or associated with particle precipitations from those formed by plasma transport and segmentation from sunlit regions. Such classification of polar patch types has not been available in literature. In this paper, we identify a new enhanced density feature in the topside *F* region ("polar cap hot patches") and show the observational differences in the characteristics of classical and hot patches in the polar cap region by using multi-instrument observations. We also show their effects on Global Navigation Satellite Systems (GNSS) signal scintillation.

2. Observations and Results

During the interval of about 22:15–22:45 UT on 30 January 2012, there were two DMSP satellites (F16 and F17) crossing the polar region at about 860 km altitude one after another in the Northern Hemisphere. Both satellites traversed the auroral oval before and after crossing the polar cap, which were determined by considering the boundaries of the particle precipitations and the flow reversal from sunward to antisunward. The plasma number density showed several small variations in the topside ionosphere in the auroral oval, especially in the dusk oval early in the pass (Figure 1a), which may be due to the sunward return flow in the dawn/dusk oval bringing the nightside low-density cold plasma and limiting the ionospheric density in auroral oval at dayside sectors. The horizontal velocity in the auroral oval is sunward with enhancements associated with the auroral arcs corresponding to the structured enhancements of precipitating energy flux in the electron spectrum (Figures 1a and 1g), while the vertical velocity was mainly upward (Figure 1b), suggesting an ion heating process [*Zhang et al.*, 2016a], which can lead to strong upward ion flux (Figure 1c). During these upflow events, the electron temperature, Poynting flux and electron and ion energy fluxes showed clear and strong enhancements with notable regions 1 and 2 field-aligned current (Figures 1d–1f), suggesting these upflows belong to auroral bulk ion upflows.

After entering the polar cap region, satellite F16 measured small enhancements of plasma density at the beginning, when the flows turned antisunward and downward with an increasing vertical flux, a decreasing region 1 field-aligned current, a slightly enhanced Poynting flux, and enhanced electron energy fluxes from the magnetosheath (Figures 1a1, 1b1, 1c1, 1d1, 1e1, 1f1, and 1g1). Afterward, F16 encountered a significantly enhanced region of ion number density, where the density was dominated by O^+ and enhanced by about a factor of three and the electron temperature slightly decreased. These are the typical plasma features of a classical polar cap patch, suggesting it is transported from dayside sunlit region [e.g., *Zhang et al.*, 2011, 2013b, 2016b]. Inside this classical polar cap patch, the ion flows were very weak and steady in antisunward and downward directions, leading to enhancements of downward O^+ flux, the ion temperature was increased to about 400 K higher than the electron temperature, the field-aligned currents and Poynting flux were approximately zero, and the electron energy fluxes were very small within energies below 1 keV. These O^+ fluxes may be mainly contributed by the downward falling heavy ions, which were originally upward accelerated by the cusp/cleft ion fountain and returned back into the polar cap due to gravity [*Lockwood et al.*, 1985a, 1985b; *Redmon et al.*, 2010; *Zhang et al.*, 2016a]. After exiting the classical patch, all parameters observed by satellite F16 remain stable except for small and variable horizontal and vertical flows. This continues until it encountered another significantly enhanced region of ion number density, where the ion density was also dominated by O^+ and enhanced by about a factor of 4 with sharper boundaries than the classical patch, and the electron temperature was clearly enhanced, suggesting this plasma was associated with particle precipitation. Notably, the density is larger than for the classical patch. In order to differentiate this from a classical patch, we call this type of irregularity a "polar cap hot patch," which is located inside the polar cap near the dawnside auroral oval. Inside the polar cap hot patch, horizontal ion flows were strongly enhanced and antisunward with strong shears, maybe associated with flow channels [*Carlson* 2012, *Nishimura et al.*, 2014], while the vertical ion flows partially turned to weakly upward, resulting in partial upward enhancements of O^+ flux. Also, the ion temperature was unstable and slightly decreased, the estimated field-aligned currents increased to downward (around the edge of region 1 field-aligned current), the Poynting flux was clearly enhanced, and the electron and ion energy fluxes showed several pulsed enhancements associated with auroral arcs generated by particle precipitation from the magnetosheath (Figures 1f1 and 1g1). Note that the ion density enhancement was much sharper with several peaks in the polar cap hot patch than the classical patch (Figure 1a1), which is clearly associated with the enhancements in the energy flux of the low-energy precipitating particles (Figures 1f1 and 1g1). Thus, we averaged the energy flux of the low-
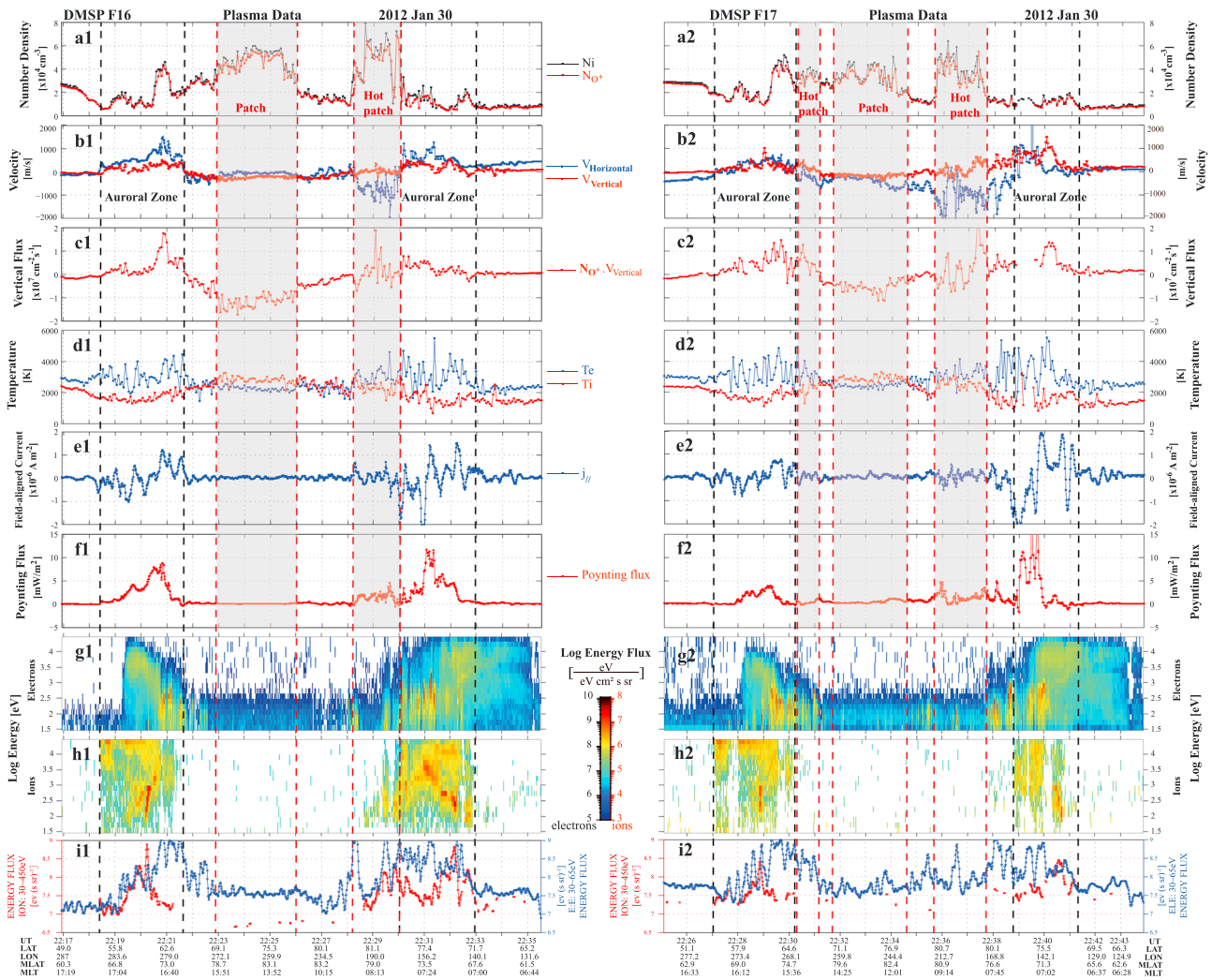
Figure 1. A time series of in situ plasma parameters measured by DMSP F16 and F17. Parameters shown are (a1 and a2) plasma number densities for O^+ and total ions, (b1 and b2) the cross-track vertical and horizontal ion flow, (c1 and c2) the vertical ion flux of thermal O^+, (d1 and d2) the ion and electron temperature, (e1 and e2) the estimated field-aligned current, $j_{//}$, (f1 and f2) the calculated Poynting flux, (g1 and g2) the electron energy flux, (h1 and h2) the ion energy flux, and (i1 and i2) the averaged energy flux for low-energy band of ions and electrons. The vertical dashed lines separate the approximate locations of the auroral zone, classical polar cap patch, and polar cap hot patch (also highlighted by the grey area), respectively.

energy bands for ions (30–450 eV) and electrons (30–65 eV), respectively, which will help us to roughly identify the contributions of low-energy particle precipitations in the classical and hot patches. From Figure 1i1, we can find the averaged energy fluxes were largely enhanced around the density peaks in the hot patch, but not in the classical patch, which further confirms the hot patch were associated with the low energy particle precipitations.

Satellite F17 entered the polar cap region about 9 min after F16 and observed a newly growing polar cap hot patch inside the polar cap just poleward of the duskside aurora oval with enhanced density, antisunward and upward flows, upward O^+ fluxes, enhanced electron temperature, slightly increased FACs and Poynting fluxes, and clearly enhanced precipitating electron energy fluxes. This may be not a mature hot patch but as the initial phase of a hot patch. Afterward, F17 also encountered a classical patch and a hot patch with similar features to those inside the classical and hot patches observed by F16. The density inside the classical and hot patches evolved and decayed by about one third from that observed by F16, where weak flows resulted in the classical patch remaining almost stopped. The hot patch, however, moved deeper into the polar cap because of the flow channels. The averaged energy fluxes were also clearly enhanced around the density peaks in the polar cap hot patch, but not in the classical patch.
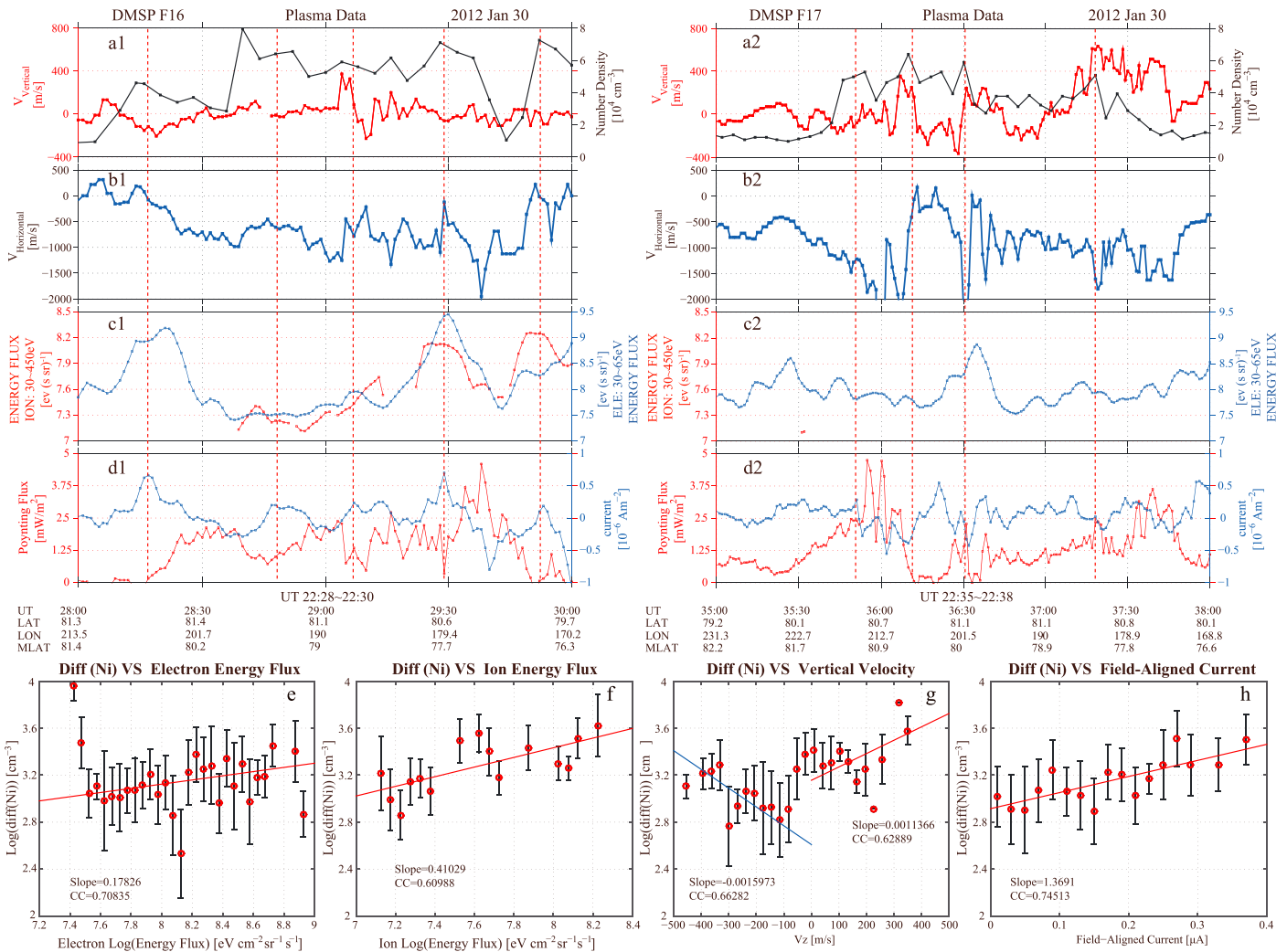
Figure 2. The detailed plasma data from the polar cap hot patch observed during the interval of 22:28–22:30 UT by DMSP F16 and of 22:35–22:38 UT by F17. Parameters shown are (a1 and a2) ion vertical velocity and number density, (b1 and b2) ion horizontal velocity, (c1 and c2) the averaged energy flux for low-energy band for ions and electrons, (d1 and d2) the estimated field-aligned current, $j_{//}$, and Poynting flux, and the averaged scatterplots with linear fitted lines (red or blue) for these periods as the differential number density versus the averaged energy flux for low-energy band for (e) electrons and (f) ions, (g) the ion vertical velocity, and (h) the field-aligned current. The red dashed lines in Figures 2a–2d highlighted the density enhancement for comparing with other parameters.

In order to further investigate the source plasma of the density enhancements inside the polar cap hot patch, we zoom in the plasma data during the interval of 22:28–22:30 UT for F16 and 22:35–22:38 UT for F17, when the satellites crossed the polar cap hot patch. Figure 2 only presents the selected plasma parameters for those intervals in the top panels to show in detail: (a1 and a2) the ion number density and vertical velocity, (b1 and b2) ion horizontal velocity, (c1 and c2) the ion and electron averaged energy flux in the low-energy band, and (d1 and d2) the estimated field-aligned current and Poynting flux. From Figures 2a–2d, we can find almost every density enhancement was associated with enhancement of low-energy particle precipitations and/or ion upflow with clear flow shear and enhancement of field-aligned current in the polar cap hot patch, which were highlighted by the red vertical dashed lines. We also averaged the selected parameters observed from both satellites for these periods to show in scatterplots with linear fitted lines in the bottom panels of Figure 2. From left to right, Figure 2 shows the differential number density against the averaged energy flux for low-energy band for (e) electrons and (f) ions, (g) the ion vertical velocity, and (h) the field-aligned current. The X axes of the scatterplots have been divided into bins of every 0.02 eV cm^{-2} sr^{-1} s^{-1} for Figures 2e and 2f, every 30 m/s for Figure 2g and every 0.02 μA for Figure 2h, and the data in each bin have been averaged with an error bar. Linear fittings have been run for each plot, excepted for Figure 2g which has been run two linear fits due to the roughly "V"-shape distributions. From Figures 2e–2h, we can find that there are good

correlations between the ion density variations and the other parameters (correlation coefficients (CC) are all larger than 0.6). Although the line slopes are not showing good linear dependences due to the different variation scales between the density and the other parameters, the clear trends show that the low-energy particle precipitations and/or ion upflows clearly contributed to the density enhancements. These clearly suggest the density enhancements in the polar cap hot patches were associated with low-energy particle precipitations and/or ion upflows due to the field-aligned current and flow shears.

3. Discussions

Figure 1 shows that the density in classical polar cap patches and polar cap hot patches can be enhanced with similar magnitude in the topside ionosphere but other observed properties are different, indicating that plasma may be partially of different origin (solar EUV produced versus precipitation produced or enhanced). In order to confirm this inference, we projected the in situ plasma parameters, observed by DMSP F17, onto a 2-D map of total electron content (TEC, the integral with height of the electron concentration, 1 TEC unit (TECU) = 10^{16} el/m^2) and global aurora images from the DMSP Special Sensor Ultraviolet Spectrographic imager (SSUSI) LBHS (Lyman-Birge-Hopfield bands of 140–150 nm) on a magnetic latitude (MLAT)/magnetic local time (MLT) grid (Figure 3) [*Thomas et al.*, 2013; *Zhang et al.*, 2013b, 2015]. The map for the crossing of F16 shows very similar features; thus, we have not presented the F16 data. Figure 3a shows the distribution of the O$^+$ density and the horizontal ion flows along the track of F17 satellite at approximately 860 km, which has been projected onto a 2-D map of TEC and convection pattern measured by Super Dual Auroral Radar Network (SuperDARN) radars. A standard two-cell convection in the polar ionosphere has been shown in the convection pattern and horizontal velocities, which is due to a predominantly steady and negative IMF B_z with a weak B_y component (resulting in an IMF clock angle varied around 180°) during the interval of interest (data not shown here). Figure 3a shows that two polar cap ionization patches in the GPS TEC data are located in the sector of North American and that the F17 satellite pass intersected one of them, which were segmented from lower latitude sunlit high-density regions in the afternoon sectors. The locations of the patches are highlighted by the blue ellipses. The satellite measured clear enhancements in the O$^+$ density with very low antisunward flows when they encountered the TEC patch (Figure 3a); unfortunately, the resolution and data coverage of the TEC map is not good enough to show the enhancements when the satellite encountered the polar cap hot patches, with clear density enhancements and strong antisunward flows. Note that the plasma density was much lower in the morning sectors than that in the afternoon sectors of the lower latitude regions, which may suggest that the photoionization plasma was much higher in the main source region for the classical patch than the hot patch.

Figure 3b also projected the O$^+$ number density along the orbit of the DMSP F17 satellite onto SSUSI LBHS auroral images. In Figure 3b, we find that there is a clear auroral arc in the polar cap just poleward of the dawnside auroral oval, when F17 crossed the old polar cap hot patch, and a small arc separated from the duskside aurora oval when F17 observed the new polar cap hot patch, although the auroral emissions associated with these arcs were weakened due to the dayglow removing process. This arc may be associated with the propagation of poleward moving auroral form (PMAFs) [e.g., *Zhang et al.*, 2010] or bending arc [e.g., *Carter et al.*, 2015]. There is no auroral emission associated with the classical polar cap patch. This indicates that the polar cap hot patch was associated with auroral arcs and particle precipitations and that the classical polar cap patch may just be transported from the dayside sunlit region. With the same order of density enhancement as classical patches, these hot patches were clearly associated with particle precipitation but may not be produced by precipitations alone. This may be because of photoionization plasma being transported into flow channels, where have low-energy particle precipitations associated with field-aligned currents and flow shears. The upflow ions generated by the associated field-aligned currents and flow shears may contribute to the ion density enhancement at the DMSP satellites altitude [*Maggiolo et al.*, 2012; *Y. Zhang et al.*, 2016]. This suggests that one cannot properly differentiate hot patches from classical patches in the polar cap region by using plasma density alone, but can do so by investigating other parameters together from multiple instrument observations. The same logic applies to the identification classical patches as well.

In order to survey the space weather effects of the classical patches and hot patches on the GNSS navigation signals, we selected two points: P1 [77°MLAT, 15MLT] around the initial phase of the polar cap hot patch and P2 [82°MLAT, 13MLT] around the classical polar cap patch (highlighted by the red stars with white edges in
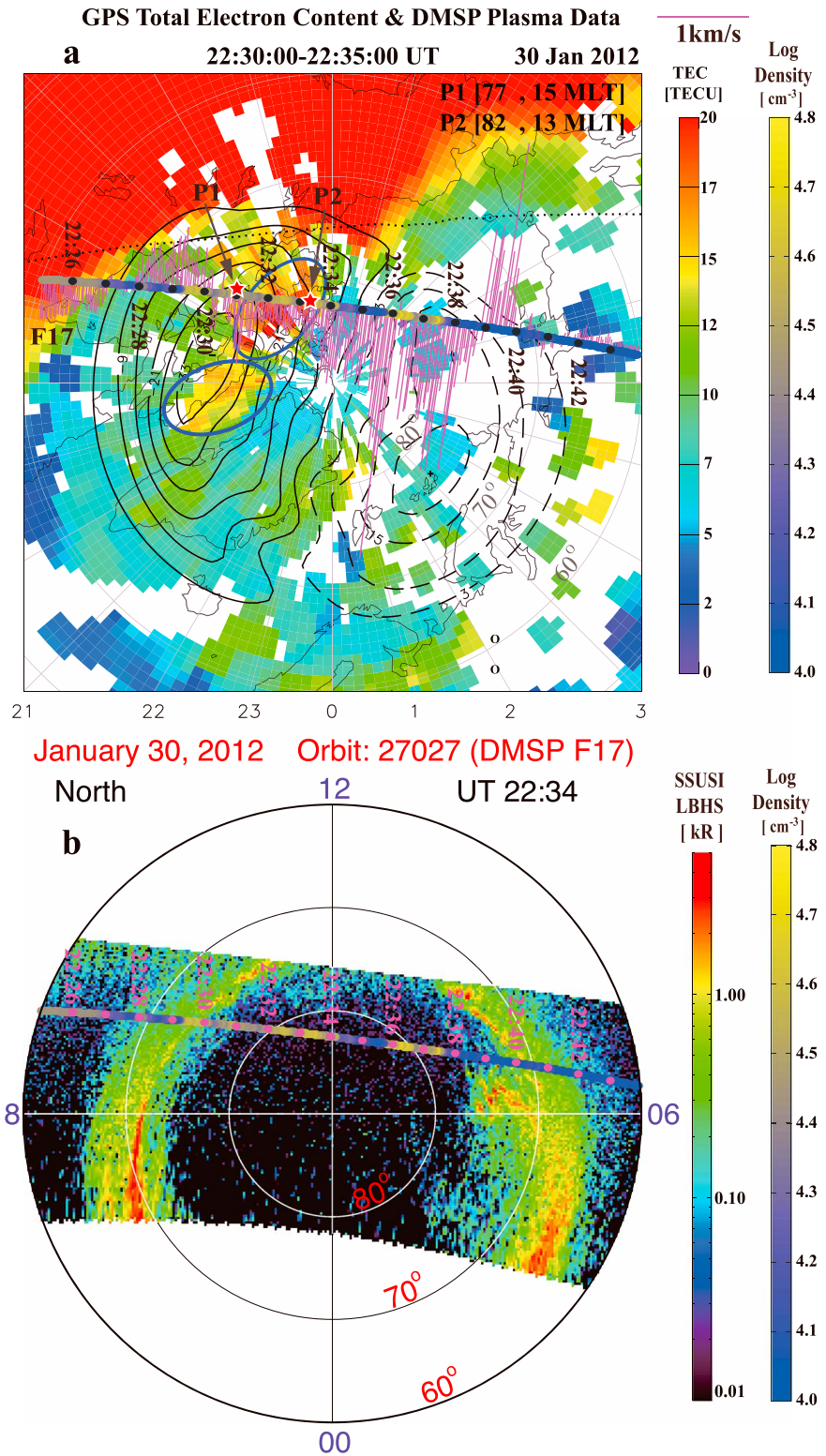
Figure 3. DMSP F17 observed in situ ion parameters projected onto the 2-D maps of median-filtered TEC and the SSUSI LBHS aurora imagers on a geomagnetic latitude (MLAT)/MLT grid [*Thomas et al.*, 2013; *Zhang et al.*, 2013b, 2015]. The projected orbit of F17 is shown by the colored thick lines, where the color scale shows the O^+ number density. The mauve drift vectors (perpendicular to the orbit) show the measured horizontal ion flows. The black dotted line across the map is the day-night terminator at 100 km altitude. The red stars with white edges in Figure 3a highlighted the selected locations of P1 [77°MLAT, 15MLT] and P2 [82° MLAT, 13MLT] for Figure 3.
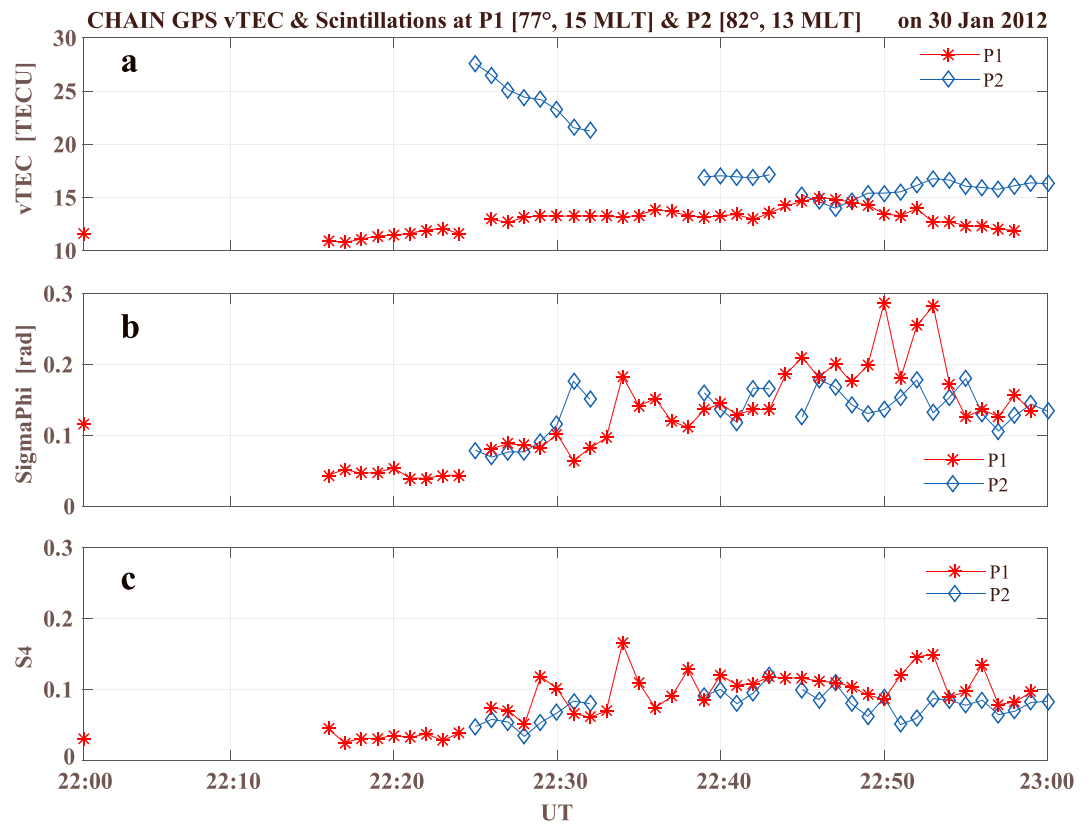
Figure 4. The calibrated vertical TEC and scintillations (σ_φ and S_4) at the Ionospheric Pierce Points (IPPs) altitude of 350 km around P1 [77°MLAT, 15MLT] and P2 [82°MLAT, 13MLT].

Figure 3a). At these two points, we extracted the time series of calibrated vertical TEC (vTEC) and scintillation data at the Ionospheric Pierce Points (IPPs) altitude of 350 km from the observations of Canadian High Arctic Ionospheric Network (CHAIN), which has 24 GPS ionospheric scintillation and TEC monitors (GISTMs), including 9 GSV4004B systems and 15 Septentrio PolarXPro systems, and locates throughout north of Canada [*Jayachandran et al.*, 2009]. In this study, four CHAIN GISTMs, located at Hall Beach [68.77°N, 278.74°E], Taloyoak (about [69.54°N, 266.44°E]), Cambridge Bay [69.10°N, 254.88°E], and Resolute [74.75°N, 265.00°E], have been used to calculate vertical TEC and scintillation data. These GISTMs received signals are from 4 GPS satellites (GPS PRN 11, 14, 17, and 32) with two satellites tracks around P1 and three tracks around P2 (see Figure S1 in the supporting information). The vertical TEC data have been processed using the methodology of *Themens et al.* [2013] and calibrated for interfrequency receiver and satellite biases by following the method proposed in *Themens et al.* [2015]. The observed scintillation data has been projected onto a grid of 1° in MLAT and 1/15 h in MLT of MLAT/MLT coordinates when the IPP was located in the grid (normally only one point located into the grid) with elevation angle above 20°. The scintillation data were then averaged in 3 × 3 grids centered at the selected points, where almost only one data grid or data gap has been taken into account during the whole interval (see Movies S1 and S2 in the supporting information). The time series of the averaged scintillation and vTEC data is presented in Figure 4. At point P1 (red lines with snowflakes in Figure 4), the vTEC only slightly and gradually enhanced by a few TECU after about 22:19 UT and reached the 15 TECU around 22:47 UT and then slightly decreased to the previous level, which were associated with the initial phase of a hot patch and the maturing phase of the hot patch, partly observed by F16 and F17, and confirmed that the hot patch may not result in the clear TEC enhancement seen in the TEC map in Figure 3. During these periods, both the amplitude and phase scintillations slightly increased when the selected point recorded the initial phase of the hot patch around 22:34 UT, while the phase scintillation (σ_φ) was largely enhanced after about 22:49 UT, which may be because the hot patch grew up and became mature one and/or be associated with a stronger presence of small-scale irregularities near the edge of the hot patch. At point P2 (blue lines with rhombuses in Figure 4), the vTEC showed decrease from 27 to 16

TECU during about 22:25–22:32 UT (at least, but ambiguous due to the data gaps), which are associated with the classical patch and its evolution and decay around the selected point partly observed by F16 and F17 satellites. During these periods, the phase scintillation (σ_φ) showed a small enhancement at the tail edge of the classical patch, but the amplitude scintillation index (S_4) stayed very low with only small variations. These observations show that phase scintillation associated with the mature polar cap hot patch was stronger than for the classical patch, which indicates that mature polar cap hot patches might result in stronger ionospheric scintillations of GNSS signals in the polar cap region than classical patches. This difference in the connection of hot patches and classical patches to scintillations in the polar cap is consistent with results in *Jin et al.* [2014, 2016] indicating that the auroral BT-1 blobs (patch + precipitation) in the auroral oval at nighttime were associated with stronger scintillations than that with a cold patch in the polar cap. Note that the TEC and scintillation data coverage (see Movies S1 and S2 in the supporting information) is still very rare, although CHAIN has 24 GNSS receivers in the northern part of Canada. Thus, more and more GNSS receivers are needed to be established in the polar regions in the near future.

4. Conclusions

We report in situ and ground-based observations of a classical patch and hot patches in the polar cap region from two polar cap crossings of the DMSP F16 and F17 satellites and GNSS receivers. These two types of irregularities originated from different sources, where the classical patch was transported from the dayside sunlit region with dense and cold plasma but the polar cap hot patches were modulated by particle precipitation and/or ion upflows. These hot patches were located inside the polar cap just poleward of the auroral zone with dense, hot plasma, and strong field-aligned currents as well as flow shears. This indicates that multi-instrument observations are necessary in identifying hot patches and classical patches. The polar cap hot patches may lead to slightly stronger ionospheric phase scintillations of GNSS signals in the polar cap region than classical patches. These observations will provide us with new insights for understanding polar cap dynamics, leading to improved space weather forecasts.

References

Basu, S., S. Basu, E. MacKenzie, W. R. Coley, J. R. Sharber, and W. R. Hoegy (1990), Plasma structuring by the gradient drift instability at high latitudes and comparison with velocity shear driven processes, *J. Geophys. Res.*, 95(A6), 7799–7818, doi:10.1029/JA095iA06p07799.

Carlson, H. C. (1994), The dark polar ionosphere: Progress and future challenges, *Radio Sci.*, 29(1), 157–165, doi:10.1029/93RS02125.

Carlson, H. C. (2012), Sharpening our thinking about polar cap ionospheric patch morphology, research, and mitigation techniques, *Radio Sci.*, 47, RS0L21, doi:10.1029/2011RS004946.

Carter, J. A., S. E. Milan, R. C. Fear, A. Kullen, and M. R. Hairston (2015), Dayside reconnection under interplanetary magnetic field B_y-dominated conditions: The formation and movement of bending arcs, *J. Geophys. Res. Space Phys.*, 120, 2967–2978, doi:10.1002/2014JA020809.

Crowley, G. (1996), Critical review of ionospheric patches and blobs, in *Review of Radio Science 1992–1996*, edited by W. R. Stone, pp. 619–648, Oxford Univ. Press, U. K.

Crowley, G., A. J. Ridley, D. Deist, S. Wing, D. J. Knipp, B. A. Emery, J. Foster, R. Heelis, M. Hairston, and B. W. Reinisch (2000), Transformation of high-latitude ionospheric F region patches into blobs during the March 21, 1990, storm, *J. Geophys. Res.*, 105(A3), 5215–5230, doi:10.1029/1999JA900357.

Foster, J. C., et al. (2005), Multiradar observations of the polar tongue of ionization, *J. Geophys. Res.*, 110, A09S31, doi:10.1029/2004JA010928.

Jayachandran, P. T., et al. (2009), Canadian High Arctic Ionospheric Network (CHAIN), *Radio Sci.*, 44, RS0A03, doi:10.1029/2008RS004046.

Jin, Y., J. I. Moen, and W. J. Miloch (2014), GPS scintillation effects associated with polar cap patches and substorm auroral activity: Direct comparison, *J. Space Weather Space Clim.*, 4, A23, doi:10.1051/swsc/2014019.

Jin, Y., J. I. Moen, and W. J. Miloch (2015), On the collocation of the cusp aurora and the GPS phase scintillation: A statistical study, *J. Geophys. Res. Space Phys.*, 120, 9176–9191, doi:10.1002/2015JA021449.

Jin, Y., J. I. Moen, W. J. Miloch, L. B. N. Clausen, and K. Oksavik (2016), Statistical study of the GNSS phase scintillation associated with two types of auroral blobs, *J. Geophys. Res. Space Phys.*, 121, 4679–4697, doi:10.1002/2016JA022613.

Knudsen, W. C. (1974), Magnetospheric convection and the high-latitude F_2 ionosphere, *J. Geophys. Res.*, 79, 1046–1055, doi:10.1029/JA079i007p01046.

Lockwood, M., and H. C. Carlson Jr. (1992), Production of polar cap electron density patches by transient magnetopause reconnection, *Geophys. Res. Lett.*, 19(17), 1731–1734, doi:10.1029/92GL01993.

Lockwood, M., et al. (2005), Motion of the dayside polar cap boundary during substorm cycles: II. Generation of poleward-moving events and polar cap patches by pulses in the magnetopause reconnection rate, *Ann. Geophys.*, 23, 3513–3532.

Lockwood, M., J. H. Waite Jr., T. E. Moore, J. F. E. Johnson, and C. R. Chappell (1985a), A new source of suprathermal O+ ions near the dayside polar cap boundary, *J. Geophys. Res.*, 90, 4099–4116, doi:10.1029/JA090iA05p04099.

Lockwood, M., M. O. Chandler, J. L. Horwitz, J. H. Waite Jr., T. E. Moore, and C. R. Chappell (1985b), The cleft ion fountain, *J. Geophys. Res.*, 90, 9736–9748, doi:10.1029/JA090iA10p09736.

MacDougall, J., and P. T. Jayachandran (2007), Polar patches: Auroral zone precipitation effects, *J. Geophys. Res.*, 112, A05312, doi:10.1029/2006JA011930.

Maggiolo, R., M. Echim, S. Wedlund, Y. Zhang, D. Fontaine, G. Lointier, and J.-G. Trotignon (2012), Polar cap arcs from the magnetosphere to the ionosphere: Kinetic modelling and observations by Cluster and TIMED, *Ann. Geophys.*, 30, 283–302, doi:10.5194/angeo-30-283-2012.

Moen, J., et al. (2006), EISCAT observations of plasma patches at sub-auroral cusp latitudes, *Ann.. Geophys.*, *24*, 2363–2374.

Nishimura, Y., et al. (2014), Day-night coupling by a localized flow channel visualized by polar cap patch propagation, *Geophys. Res. Lett.*, *41*, 3701–3709, doi:10.1002/2014GL060301.

Oksavik, K., C. van der Meeren, D. A. Lorentzen, L. J. Baddeley, and J. Moen (2015), Scintillation and loss of signal lock from poleward moving auroral forms in the cusp ionosphere, *J. Geophys. Res. Space Phys.*, *120*, 9161–9175, doi:10.1002/2015JA021528.

Redmon, R. J., et al. (2010), Vertical thermal O^+ flows at 850 km in dynamic auroral boundary coordinates, *J. Geophys. Res.*, *115*, A00J08, doi:10.1029/2010JA015589.

Themens, D. R., P. T. Jayachandran, R. B. Langley, J. W. MacDougall, and M. J. Nicolls (2013), Determining receiver biases in GPS-derived total electron content in the auroral oval and polar cap region using ionosonde measurements, *GPS Solutions*, *17*(3), 357–369.

Themens, D. R., P. T. Jayachandran, and R. B. Langley (2015), The nature of GPS differential receiver bias variability: An examination in the polar cap region, *J. Geophys. Res. Space Phys.*, *120*, 8155–8175, doi:10.1002/2015JA021639.

Thomas, E. G., J. B. H. Baker, J. M. Ruohoniemi, L. B. N. Clausen, A. J. Coster, J. C. Foster, and P. J. Erickson (2013), Direct observations of the role of convection electric field in the formation of a polar tongue of ionization from storm enhanced density, *J. Geophys. Res. Space Physics*, *118*, 1180–1189, doi:10.1002/jgra.50116.

Wang, Y., Q. -H. Zhang, P. T. Jayachandran, M. Lockwood, S.-R. Zhang, J. Moen, Z.-Y. Xing, Y.-Z. Ma, and M. Lester (2016), A comparison between large-scale irregularities and scintillations in the polar ionosphere, *Geophys. Res. Lett.*, *43*, 4790–4798, doi:10.1002/2016GL069230.

Weber, E. J., et al. (1984), *F* layer ionization patches in the polar cap, *J. Geophys. Res.*, *89*(A3), 1683–1694, doi:10.1029/JA089iA03p01683.

Zhang, Q.-H., et al. (2010), Simultaneous observations of reconnection pulses at Cluster and their effects on the cusp aurora observed at the Chinese Yellow River Station, *J. Geophys. Res.*, *115*, A10237, doi:10.1029/2010JA015526.

Zhang, Q. -H., et al. (2011), On the importance of interplanetary magnetic field $|B_y|$ on polar cap patch formation, *J. Geophys. Res.*, *116*, A05308, doi:10.1029/2010JA016287.

Zhang, Q.-H., et al. (2013a), Polar cap patch segmentation of the tongue of ionization in the morning convection cell, *Geophys. Res. Lett.*, *40*, 2918–2922, doi:10.1002/grl.50616.

Zhang, Q. -H., et al. (2013b), Direct observations of the evolution of polar cap ionization patches, *Science*, *339*, 1597–1600, doi:10.1126/science.1231487.

Zhang, Q. H., et al. (2015), Direct observations of the full Dungey convection cycle in the polar ionosphere for southward interplanetary magnetic field conditions, *J. Geophys. Res. Atmos*, *120*, 4519–4530, doi:10.1002/2015JA021172.

Zhang, Q. -H., et al. (2016a), Earth's ion upflow associated with polar cap patches: Global and in situ observations, *Geophys. Res. Lett.*, *43*, 1845–1853, doi:10.1002/2016GL067897.

Zhang, Q.-H., et al. (2016b), Polar cap patch transportation beyond the classic scenario, *J. Geophys. Res. Space Physics*, *121*, 9063–9074, doi:10.1002/2016JA022443.

Zhang, Y., L. J. Paxton, Q. Zhang, and Z. Xing (2016), Polar cap arcs: Sun-aligned or cusp-aligned?, *J. Atmos. Sol. Terr. Phys.*, *146*, 123–128.

Zou, Y., et al. (2016), Localized field-aligned currents in the polar cap associated with airglow patches, *J. Geophys. Res. Space Physics*, *121*, 10,172–10,189, doi:10.1002/2016JA022665.